Geochemical characteristics and reasons for the carbon isotopic reversal of natural gas in the southern Jingbian gas field, Ordos Basin, China

Authors for correspondence:
Wenxue Han, Xiangchun Chang, and
Weijiao Ma, Emails: vincerham@qq.com;
xcchang@sina.com; maweijiao_cug@126.com

Wenxue Han[1,2] , Xiangchun Chang[1,2], Weijiao Ma[3], Shizhen Tao[4], Jingli Yao[5], Lianhua Hou[4] and Weiwei Yang[5]

[1]College of Earth Science and Engineering, Shandong University of Science and Technology, Qingdao 266590, China; [2]Laboratory for Marine Mineral Resources, Qingdao National Laboratory for Marine Science and Technology, Qingdao 266071, China; [3]School of Earth and Space Sciences, Peking University, Beijing 100871, China; [4]Research Institute of Petroleum Exploration and Development, PetroChina, Beijing 100083, China and [5]Exploration and Development Research Institute of PetroChina Changqing Oilfield Company, Xi'an, Shaanxi 710021, China

Abstract

The carbon isotope value of ethane in the southern part of the Jingbian gas field is lower than that in the northern part, indicating a carbon isotopic reversal in the southern Jingbian gas field ($\delta^{13}C_{methane} > \delta^{13}C_{ethane}$). Through comparing the geochemical characteristics of gases in the southern and northern parts of the gas field, the reasons for the carbon isotopic reversal in the southern Jingbian gas field were determined to be high thermal maturity and mixing action. When thermal maturity reaches a critical value, the carbon isotope value of ethane becomes relatively more depleted with thermal maturity. Although the carbon isotope value of methane increases with thermal maturity, the extent is relatively smaller. Finally, the rare phenomenon of $\delta^{13}C_{methane} > \delta^{13}C_{ethane}$ occurs. High thermal maturity leads to the secondary thermal cracking of gases. Mixing of the cracked gases and primary gases also leads to carbon isotopic reversal. Both of the above mechanisms share a common premise, which is high thermal maturity.

1. Introduction

The Ordos Basin is one of the main natural gas producing areas in China. Several giant gas fields have been discovered in the basin including the Sulige, Yulin, Wushenqi, Zizhou, Mizhi, Shenmu, Daniudi, Dongsheng and Jingbian (Huang *et al.* 2015; Dai *et al.* 2016*b*; Wang *et al.* 2016; Fan *et al.* 2019). It is widely accepted that natural gas in these gas fields, except for the Lower Palaeozoic Jingbian gas field, is generated from the Carboniferous–Permian coal measure strata (Liu *et al.* 2009, 2016; Han *et al.* 2017*a*; Lv *et al.* 2017; Wu *et al.* 2017). The controversy over the origins of the natural gas in the Lower Palaeozoic Jingbian gas field is due to the abnormal geochemical characteristics of the natural gas (Li *et al.* 2008; Liu *et al.* 2009; Han *et al.* 2017*a*; Wang *et al.* 2017*b*).

When carbon isotope values increase with an increase in carbon numbers in alkane gases, it is described as a positive series ($\delta^{13}C_{methane} < \delta^{13}C_{ethane} < \delta^{13}C_{propane} < \delta^{13}C_{butane}$). This is usually characteristic of organic gases. When the carbon isotope series is the opposite ($\delta^{13}C_{methane} > \delta^{13}C_{ethane} > \delta^{13}C_{propane} > \delta^{13}C_{butane}$), it is described as a negative or full reversal series and is usually characteristic of inorganic gases (Dai *et al.* 2004, 2016*a*; Li *et al.* 2018). However, if carbon isotope values appear in neither of the abovementioned series, but are arranged in a disordered form, it is described as a partial carbon isotopic reversal. The carbon isotope values of the Lower Palaeozoic Jingbian gas field show a partial reversal, and this is why the origins of the natural gas in the Lower Palaeozoic Jingbian gas field are controversial (Li *et al.* 2008; Liu *et al.* 2009; Han *et al.* 2017*a*; Wang *et al.* 2017*b*).

In summary, a carbon isotopic reversal is mainly caused by the following mechanisms:

(1) Mixing action, which refers to the mixing of organic and inorganic alkanes, coal-derived gas and oil-derived gas, and gases with 'identical type and different sources' or 'identical sources in different periods' (Dai *et al.* 2004, 2016*a*; Zou *et al.* 2018);
(2) Fractionation, which includes migration fractionation and water-solution fractionation (Zhang & Krooss, 2001; Xiao, 2012);
(3) High thermal maturity (Fuex, 1977; Tilley & Muehlenbachs, 2013; Xia *et al.* 2013);
(4) Bacterial oxidation, oxidation–reduction reactions with transition metals and water or thermochemical sulfate reduction (TSR) (Burruss & Laughrey, 2010; Zumberge *et al.* 2012; Liu *et al.* 2013).
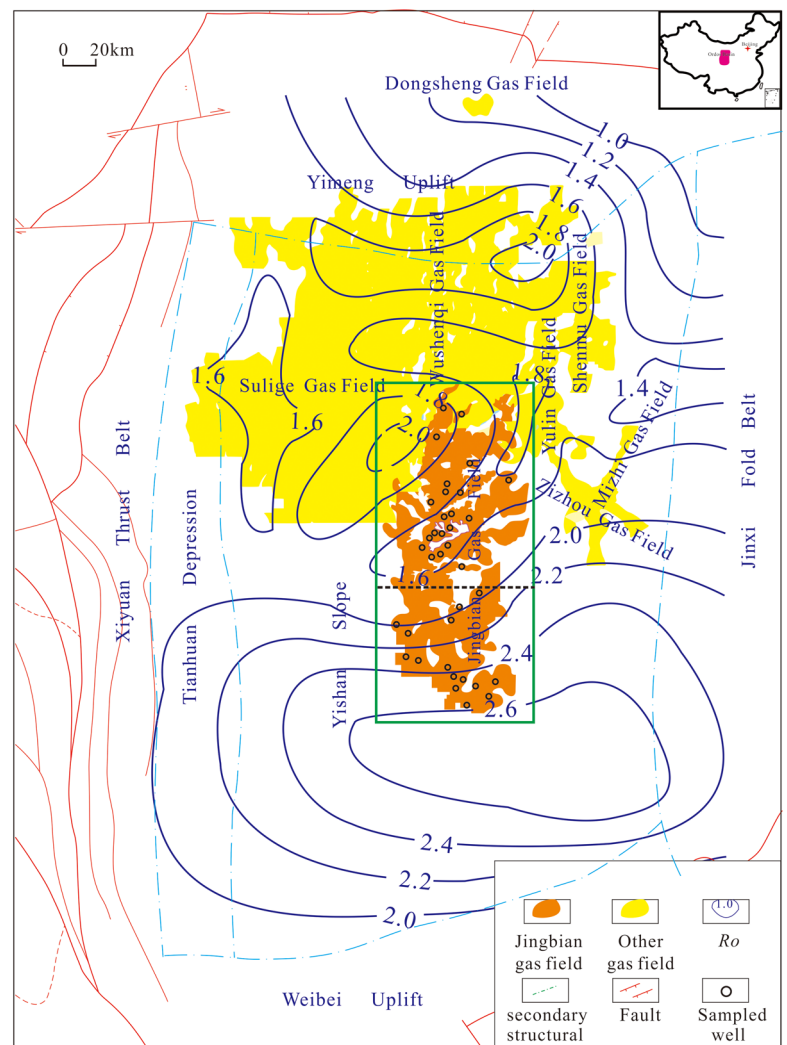
Fig. 1. (Colour online) Contour map of R_o values and geological tectonics in the Ordos Basin, China (modified after Dai *et al.* 2016*a*).

As mentioned above, the reason for the carbon isotopic reversal is still unclear, which leads to the dispute over the origins of the natural gas in the Lower Palaeozoic Jingbian gas field (Li *et al.* 2008; Liu *et al.* 2009; Han *et al.* 2017*a*; Wang *et al.* 2017*b*). Therefore, it is necessary to study the reasons for the carbon isotopic reversal.

The natural gas shows a carbon isotopic reversal in the southern Jingbian gas field, which has a higher thermal maturity. Comparative study of the geochemical characteristics of the natural gas in the southern and northern parts of the Jingbian gas field has rarely been carried out, but it can help to identify the impacts of thermal maturity on natural gas. Moreover, such a comparative study can cover the whole Jingbian gas field, avoiding the drawbacks of previous studies that only focused on either the southern or northern parts of the Jingbian gas field (Li *et al.* 2008; Liu *et al.* 2009, 2016; Wang *et al.* 2017*b*).

2. Geologic setting

The Ordos Basin has an Archaean and Proterozoic metamorphic crystalline basement covered by Mesoproterozoic, Neoproterozoic, Palaeozoic, Mesozoic and Cenozoic sediments with an average thickness of ~6000 m (Ding *et al.* 2016; Dai *et al.* 2016*b*; Yang *et al.* 2017; Fan *et al.* 2018; Du *et al.* 2019). The Lower Palaeozoic strata are mainly

marine carbonates, and the Upper Palaeozoic–Mesozoic strata are mainly terrestrial clastic rocks (Dai *et al.* 2016*b*). The Ordos Basin can be divided into six tectonic units, i.e. the Yimeng Uplift, Weibei Uplift, Jinxi Fold Belt, Xiyuan Thrust Belt, Yi-Shaan Slope and Tianhuan Depression (Liu *et al.* 2009; Yang *et al.* 2014; Han *et al.* 2017*b*; Li *et al.* 2017; Shi *et al.* 2019) (Fig. 1). The Lower Palaeozoic Jingbian gas field, located in the central Yi-Shaan Slope, extends in a N–S direction with a large longitudinal span (Dai *et al.* 2016*b*; Xu *et al.* 2016; Zhou *et al.* 2016).

All the reservoirs of the gas fields in the Ordos Basin are Upper Palaeozoic terrestrial clastic rocks, except for the Jingbian gas field, which is mainly produced from the Lower Palaeozoic marine carbonate (Li *et al.* 2008; Liu *et al.* 2009, 2016; Han *et al.* 2017*a*). The source rocks are mainly Carboniferous–Permian coal measure strata (Dai *et al.* 2016*b*; Han *et al.* 2017*a*; Lv *et al.* 2017; Wu *et al.* 2017). In the Lower Palaeozoic Jingbian gas field, the gas reservoirs correspond to the Carboniferous Benxi Formation aluminous mudstone with continental argillaceous rocks as the cap rocks; laterally, they are sealed by the Ordovician clayey gypsum dolomite (Li *et al.* 2008; Liu *et al.* 2009, 2016; Dai *et al.* 2016*b*; Han *et al.* 2017*a*).

In this paper, the Jingbian gas field is divided into southern and northern parts based on thermal maturity in order to analyse the effect of thermal maturity on the carbon isotopes. The Jingbian gas

field is adjacent to the Sulige, Wushenqi, Daniudi, Yulin, Dongsheng and Shenmu gas fields in the north and the Zizhou and Mizhi gas fields in the northeast (Li *et al.* 2008; Liu *et al.* 2009; Dai *et al.* 2016*b*; Han *et al.* 2017*a*). The southern part of the Jingbian gas field has a much higher thermal maturity than the northern part and does not border other gas fields (Fig. 1). Exploration of the Jingbian gas field has increased recently, with many wells being drilled in the southern part.

The geothermal gradient and terrestrial heat flow values for the southern Ordos Basin are obviously larger than those of the northern Ordos Basin (Ren *et al.* 2017). The difference indicates that the southern part has a higher degree of thermal evolution and thermal anomalies. The reason for such a difference is that in early Cretaceous time, thermal activity in the deep lithosphere of the Ordos Basin increased, and the thermal activity in the southern Ordos Basin was much stronger than that in the northern part (Ren *et al.* 2007). The abnormal degree of thermal evolution in the southern Ordos Basin has something to do with the intensive tectonic activity of the Qinling orogenic belt during the late Yanshan period. The intense intra-continental orogeny and intra-continental subduction during the Yanshan period may have caused the mantle uplift in the southern Ordos Basin, resulting in an abnormal geothermal field (Ren *et al.* 2006; He & Zhang, 2018).

During the middle and late Yanshan Movement, accompanied by strong orogenic movement around the Ordos Basin, volcanic activity was frequent in the south. Nepheline syenite was discovered in Well Long 1 with a thickness of 154.6 m, and magmatic rock was found in Well Long 2 with a thickness of 384.5 m in the southern area (Ren *et al.* 2006). This indicates that volcanic activity occurred in the southern region, which directly leads to the higher thermal maturity in the southern region than in the northern region. K-bentonite was discovered in the south, which also provides evidence for volcanic-magmatic activity events in the southern region (Wang *et al.* 2015). In the south, a large number of tuffs were also developed, indicating that the crater may be in the Qinling orogenic belt adjacent to the southern part of the basin (Zhang *et al.* 2009). Seismic sections and gravity and magnetic anomalies through the south also prove that there are magmatic rocks buried in the deep part of the south (Zhang *et al.* 1985; Zhang, 1989).

The results of simulation of the geothermal history of the basin suggest that the palaeo-geothermal gradient in late Mesozoic time is higher, and the palaeo-geothermal gradient in the south is higher than that in the north, with abnormally high values appearing in the south (Ren *et al.* 2006, 2007). The thermal structure of the sedimentary layers in the south and north of the basin is quite different, and the temperature at the bottom of each layer in the south is higher than that in the north. The degree of thermal evolution gradually increases from north to south, and the sediments enter the over-mature stage in the south Jingbian gas field (Yang *et al.* 2012; Feng *et al.* 2016).

The south Jingbian gas field was a depositional centre with maximum burial in late Palaeozoic time (Feng *et al.* 2016). The south contains sandstone reservoirs interbedded with shale of higher thermal maturity (Li *et al.* 2015). This assemblage provided favourable conditions for the cracked gas to migrate to the sandstone reservoir in the south Jingbian gas field (Wu *et al.* 2015).

3. Samples and methods

Twenty-one gas samples were analysed from the northern part and 15 gas samples were collected from the southern part of the Jingbian gas field. The northern gas sample data were compiled

from the literature (Dai *et al.* 2016*b*), and the southern gas samples were collected and analysed in this study.

These gas samples were collected in high-pressure cylinders (pressure resistant up to 15 MPa) at pressures of ~5 MPa after the vessels had been repeatedly flushed and refilled. Measurements of components and carbon isotope values were conducted at the PetroChina Research Institute of Petroleum Exploration and Development (RIPED) in Beijing, China. To determine the components of the natural gas, an Agilent HP7890A gas chromatograph (GC) was equipped with a flame ionization detector and a thermal conductivity detector. The GC oven temperature started at 30 °C for 10 min, and then rose to the maximum (i.e. 180 °C) at 10 °C/min and was maintained for 20–30 min. A capillary column was used to separate single gas hydrocarbon compositions (PLOT Al_2O_3, 50 m × 0.53 mm).

A mass spectrometer (Finnigan MAT Delta S) was used to analyse the carbon isotopes. The temperature started at 33 °C, then rose from 33 °C to 80 °C at 8 °C/min, then to 250 °C at 5 °C/min, where it was held for 10 minutes. Each gas sample was measured three times and averaged, yielding an analytical precision of ±0.3 ‰.

The carbon isotope values of natural gases have been established by many scholars before (Dumke *et al.* 1989; Coplen *et al.* 2006), but owing to many years of distribution, the international reference materials are almost exhausted. Therefore, new standard materials for carbon isotope measurement of natural gases should be established (Dai *et al.* 2012; Huang *et al.* 2015). The international standard materials NG-1 (coal-derived gas), NG-2 (biogas) and NG-3 (oil-derived gas), which were co-developed by China and laboratories from the USA and Germany (Dai *et al.* 2012), were employed for the carbon isotope analysis. The calibrated values of the NG-1, NG-2 and NG-3 standards are as follows:

$$NG - 1 :$$
$$\delta^{13}C_{methane} = -34.18 \pm 0.10‰, \delta^{13}C_{ethane} = -24.66 \pm 0.11‰,$$
$$\delta^{13}C_{propane} = -22.21 \pm 0.11‰, \delta^{13}C_{i-butane} = -21.62 \pm 0.12‰,$$
$$\delta^{13}C_{n-butane} = -21.74 \pm 0.13‰, \delta^{13}C_{carbon\ dioxide} = -5.00 \pm 0.12‰$$

$$NG - 2 :$$
$$\delta^{13}C_{methane} = -68.89 \pm 0.12‰$$

$$NG - 3 :$$
$$\delta^{13}C_{methane} = -43.61 \pm 0.09‰, \delta^{13}C_{ethane} = -40.24 \pm 0.10‰,$$
$$\delta^{13}C_{propane} = -33.79 \pm 0.09‰$$

The carbon isotope values of the natural gases were measured on-line. Results are reported in the δ notation in per mil (‰) relative to the Vienna Pee Dee Belemnite (VPDB).

4. Results

4.a. Natural gas components

The geochemical parameters of the natural gas are listed in Table 1. Gas components are expressed in vol. % in this paper. Gases in both the southern and northern parts of the Jingbian gas field are dominated by methane, with relatively lower proportions of heavy hydrocarbon gas (heavy hydrocarbon gas means alkane

Table 1. Components and carbon isotope values of natural gas from the northern and southern parts of the Jingbian gas field

Gas field	Well	Strata	Ro	Component/%							δ¹³C/‰, VPDB				Data Sources
				CH_4	C_2H_6	C_3H_8	iC_4	nC_4	N_2	CO_2	CH_4	C_2H_6	C_3H_8	C_4H_{10}	
Northern Jingbian	S277	$O_1m_5^{1-3}$	1.77	94.41	1.76	0.36	0.05	0.03	0.72	2.96	−32.4	−25.3	−24.5	−21.1	Dai *et al.* (2016*b*)
	S193	$O_1m_5^{1-2}$	1.75	94.15	0.71	0.10	0.01	0.01	0.21	4.76	−32.8	−31.9	−29.3	−24.4	
	S155	$O_1m_5^1$	1.66	92.88	0.69	0.09	0.01	0.01	0.22	5.95	−32.7	−30.2	−27.8	-	
	S190	$O_1m_5^1$	1.78	92.90	0.64	0.07	0.01	0.01	0.20	5.40	−33.0	−29.6	−27.1	−23.3	
	S20	$O_1m_5^{1-3}$	1.61	93.10	0.30	0.16	0.01	0.02	1.02	0.55	−34.6	−31.0	−27.5	−22.1	
	S45	$O_1m_5^{1-4}$	1.63	94.92	0.16	0.04	0.00	0.00	0.25	4.44	−33.5	−30.6	−22.9	−22.5	
	S84	$O_1m_5^1$	1.62	92.40	0.81	0.12	0.01	0.01	0.99	5.09	−31.8	−28.5	−24.2	−20.9	
	S8	O_1m_5	1.64	94.96	0.94	0.12	0.02	0.01	0.40	3.42	−35.0	−28.3	−26.0	-	
	S28	$O_1m_5^2$	1.62	95.96	0.75	0.09	0.01	0.01	-	-	−34.1	−28.3	−27.3	−24.1	
	L1	O_1m_5	1.60	94.16	0.66	0.10	0.01	0.01	3.45	1.51	−33.7	−27.8	−25.6	-	
	S61	$O_1m_5^{1-2}$	1.72	97.50	0.77	0.10	0.01	0.01	-	-	−34.0	−27.7	−28.4	−24.8	
	SC1	$O_1m_5^{1-3}$	1.61	93.33	0.67	0.08	0.01	0.01	3.19	2.71	−33.9	−27.6	−26.0	−22.9	
	S74	$O_1m_5^{1-2}$	1.62	94.27	0.99	0.13	0.02	0.01	0.10	4.43	−33.4	−27.4	−25.9	−22.1	
	L5	$O_1m_5^4$	1.66	94.46	0.37	0.03	0.00	0.00	2.54	0.10	−33.0	−27.3	−26.0	−21.8	
	S58	$O_1m_5^1$	1.64	94.13	1.09	0.13	0.02	0.02	0.12	4.43	−33.9	−26.9	−27.3	−23.0	
	S227	$O_1m_5^1$	1.61	93.58	1.27	0.14	0.02	0.02	0.13	4.70	−33.8	−26.5	−26.5	−22.7	
	S2	O_1m_5	1.67	96.19	0.82	0.00	0.03	0.01	-	-	−35.9	−26.5	-	-	
	L2	$O_1m_5^3$	1.63	95.34	1.40	0.18	0.02	0.03	0.39	2.62	−35.2	−25.9	−25.4	−23.8	
	S34	$O_1m_5^1$	1.70	94.02	1.28	0.15	0.04	0.02	4.11	0.36	−35.3	−25.5	−24.4	−21.9	
	S12	$O_1m_5^{1-4}$	1.76	96.79	0.78	0.10	0.01	0.01	0.63	1.65	−34.2	−25.5	−26.4	−20.7	
	S41	$O_1m_5^1$	1.73	91.51	0.66	0.15	0.01	0.02	0.64	5.03	−33.4	−24.6	−25.0	−22.1	
Southern Jingbian	S107	$O_1m_5^{1-2}$	2.33	96.93	0.35	0.04	0.00	0.01	0.24	2.43	−31.0	−37.4	−32.9	−34.9	This study
	S310	O_1m_5	2.01	94.71	0.19	0.01	0.00	0.00	1.50	3.58	−35.2	−34.3	−27.9	-	
	S389	$O_1m_5^{1-4}$	2.29	91.14	0.40	0.06	0.01	0.01	2.45	5.93	−33.5	−35.8	−30.2	-	
	S15	$O_1m_5^{1-3}$	2.32	93.81	0.47	0.13	0.02	0.02	2.12	3.43	−31.6	−37.3	−29.4	-	
	S339	$O_1m_5^{1-2}$	2.28	93.35	0.59	0.10	0.02	0.02	2.58	3.34	−29.1	−34.2	-	-	
	S283	$O_1m_5^{1-4}$	2.21	92.37	0.30	0.03	0.00	0.00	1.37	5.93	−32.7	−33.6	−25.6	-	
	S316	$O_1m_5^{1-2}$	2.59	95.86	0.27	0.03	0.00	0.00	1.05	2.80	−32.9	−36.5	-	-	
	S434	$O_1m_5^{1-2}$	2.03	92.78	0.35	0.03	0.00	0.00	2.76	4.07	−31.6	−35.8	−30.6	-	
	S438	$O_1m_5^{1-3}$	2.07	94.92	0.41	0.04	0.00	0.00	0.63	3.99	−31.7	−37.8	−33.3	-	
	S439	$O_1m_5^{1-3}$	2.52	92.56	0.37	0.08	0.00	0.00	2.08	4.90	−32.9	−32.5	−27.3	-	
	S441	$O_1m_5^{2-3}$	2.53	85.06	0.21	0.04	0.02	0.03	0.00	14.65	−32.3	−36.8	−29.7	-	
	S279	$O_1m_5^{1-2}$	2.48	79.63	0.29	0.04	0.00	0.00	13.78	6.25	−32.2	−33.8	−27.4	−31.7	
	S303	$O_1m_5^{1-2}$	2.57	86.03	0.19	0.03	0.02	0.02	0.00	13.72	−32.2	−36.8	−29.7	-	
	S292	$O_1m_5^4$	2.50	90.87	0.24	0.03	0.00	0.00	4.04	4.82	−31.8	−33.5	−30.0	-	
	S127	$O_1m_5^4$	2.16	84.28	0.19	0.01	0.00	0.00	8.11	7.41	−32.7	−35.7	−30.6	-	

gas with a carbon number greater than 1; in this study it refers to C_2H_6–C_4H_{10}) and non-hydrocarbon gas.

The content of heavy hydrocarbon gas is 0.20–2.21 % (0.98 % on average) in the northern part of the Jingbian gas field and 0.20–0.73 % (0.38 % on average) in the southern part of the Jingbian gas field. The south is much lower than that of the north. In other words, the distribution range of the south (0.20–0.73 %) is a subset of the north (0.20–2.21 %). It is worth noting that the content of ethane is 0.16–1.76 % (0.83 % on average) in the northern part and 0.19–0.59 % (0.32 % on average) in the southern part, revealing that the north is almost 2.6 times greater than the south in terms of the average value (Fig. 2). The content of C_2H_6 and C_3H_8 in the
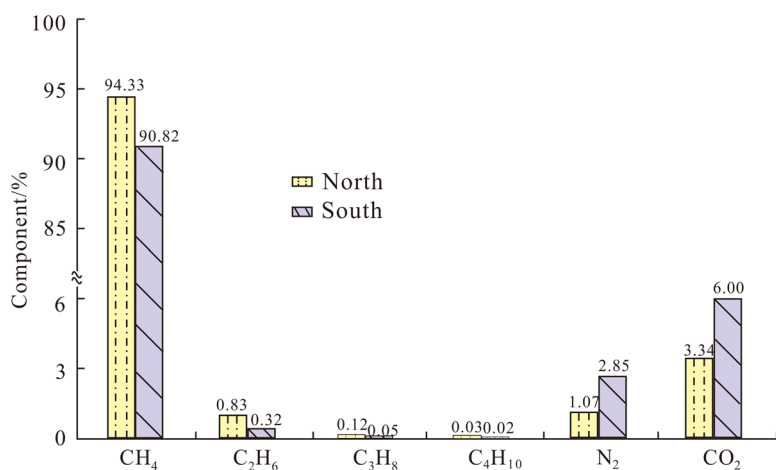
Fig. 2. (Colour online) Average gas components of natural gas in the northern and southern Jingbian gas field, Ordos Basin (data from Table 1).
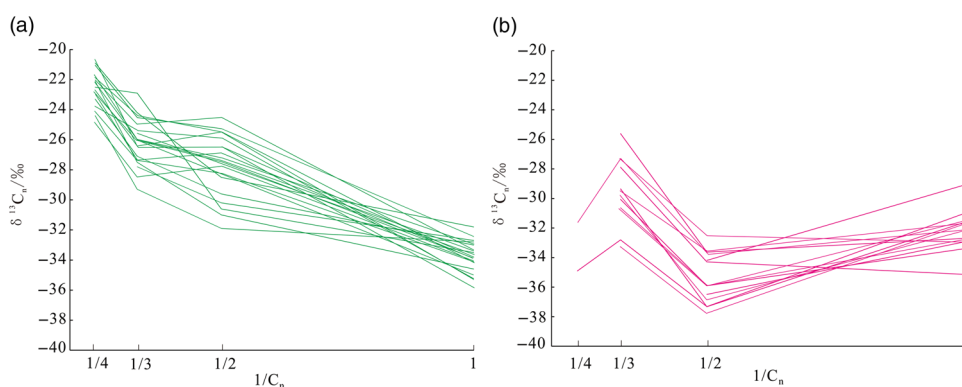
Fig. 3. (Colour online) Relationship between carbon number $1/C_n$ and $\delta^{13}C_n$ values of natural gas in the northern and southern Jingbian gas field: (a) northern Jingbian gas field; (b) southern Jingbian gas field (data from Table 1).

north is obviously higher than that in the south. The content of C_4H_{10} (including *i*-C4 and *n*-C4) in the north can be detected and measured; however, most of the content of C_4H_{10} in the south is zero. Owing to the relatively higher thermal maturity in the south, the heavy hydrocarbon was cracked, leading to the lower content of heavy hydrocarbon in the south compared with the north.

The CO_2 content is higher than in some basins. The $^3He/^4He$ ratio of noble gas in the Jingbian gas field is $3.49–6.71 \times 10^{-8}$, indicating a crustal source origin (Dai *et al.* 2016*b*). The carbon isotope values of CO_2 range from −4.6 ‰ to −0.4 ‰, which is much larger than the critical value (−8 ‰) of inorganic CO_2 (Dai *et al.* 1996), suggesting an inorganic origin. A relatively thick limestone unit was developed in the Benxi (C_2b) and Taiyuan (P_1t) formations in the area, and it is likely that CO_2 was the product of thermal cracking of these inorganic carbonates (Feng *et al.* 2016). The CO_2 content of the north ranges from 0.1 % to 5.95 %, with an average value of 3.34 %. The CO_2 content of the south ranges from 2.43 % to 14.65 %, with an average value of 5.82 %. The CO_2 content of the north is a subset of the south. Because the thermal maturity of the south is higher than that of the north, the thermal cracking of inorganic carbonates in the south produced more carbon dioxide than in the north.

4.b. Carbon isotope compositions

The $\delta^{13}C_{methane}$ values range from −35.9 ‰ to −31.8 ‰ with an average of −33.8 ± 0.10 ‰ in the northern part of Jingbian gas field,

and from −35.2 ‰ to −29.1 ‰ with an average of −32.2 ± 0.10 ‰ in the southern part of Jingbian gas field. The $\delta^{13}C_{ethane}$ values range from −31.9 ‰ to −24.6 ‰ with an average of −27.8 ± 0.11 ‰ in the northern part of Jingbian gas field, and from −37.8 ‰ to −32.5 ‰ with an average of −35.5 ± 0.11 ‰ in the southern part of Jingbian gas field. For the northern and southern parts, the interval and mode of the $\delta^{13}C_{methane}$ values are similar, but the $\delta^{13}C_{ethane}$ values are different. The $\delta^{13}C_{ethane}$ values in the southern part are much lower than those in the northern part. Moreover, a carbon isotopic reversal, namely $\delta^{13}C_{methane} > \delta^{13}C_{ethane} < \delta^{13}C_{propane}$, occurs in the southern part of Jingbian gas field, while a positive carbon isotope series, namely $\delta^{13}C_{methane} < \delta^{13}C_{ethane} < \delta^{13}C_{propane}$, is dominant in the northern part of Jingbian gas field.

A line chart of carbon isotope values, which can directly show the carbon isotopic reversal, is widely used to identify the origins of natural gas. There is a linear relationship between the carbon isotopes and the reciprocal of the compositions of thermogenic gases generated from the same source rocks (Chung *et al.* 1988; Rooney *et al.* 1995). According to the line chart of carbon isotope values (Fig. 3), the $\delta^{13}C_{methane}$ values of the northern and southern parts distribute almost in the same interval and mode with no obvious difference. However, the $\delta^{13}C_{ethane}$ values are different, being much lighter in the southern part. It can be seen from the chart that the carbon isotope values in the southern Jingbian gas field have reversed ($\delta^{13}C_{methane} > \delta^{13}C_{ethane} < \delta^{13}C_{propane}$) compared with the northern part.
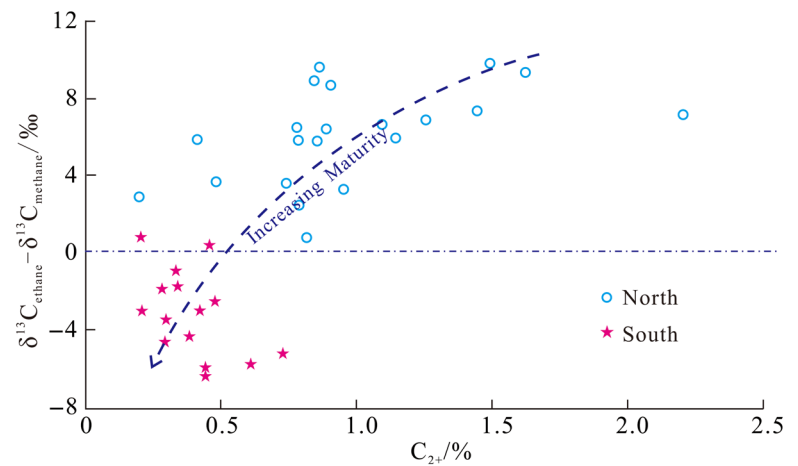
Fig. 4. (Colour online) Relationship between heavy hydrocarbon (C_{2+}) and $\delta^{13}C_{ethane} - \delta^{13}C_{methane}$ of natural gas in the northern and southern Jingbian gas field (data from Table 1).
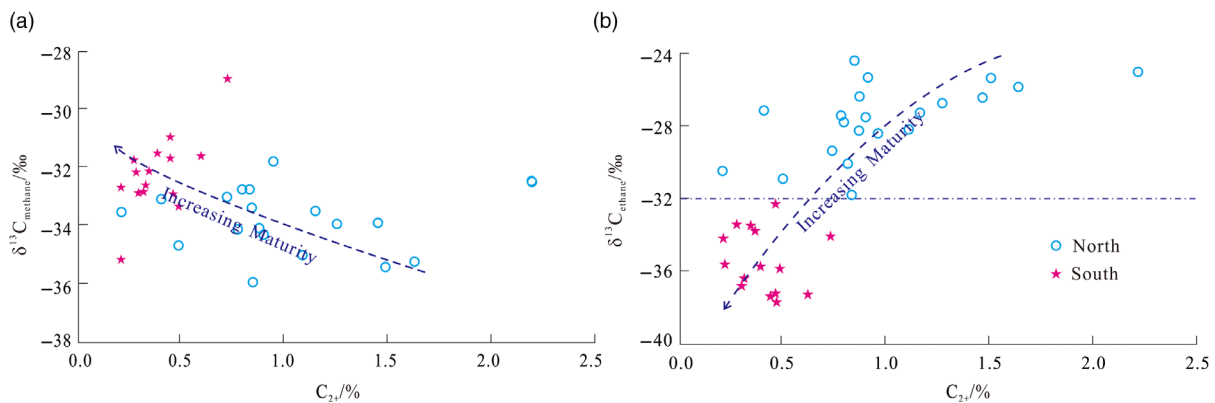
Fig. 5. (Colour online) Relationship between heavy hydrocarbon (C_{2+}) and $\delta^{13}C_n$ values of natural gas in the northern and southern Jingbian gas field (data from Table 1). (a) $\delta^{13}C_{methane}$ versus C_{2+}; (b) $\delta^{13}C_{ethane}$ versus C_{2+}.

5. Discussion

5.a. High thermal maturity

The relationship between the content of heavy hydrocarbons (C_{2+}) and the $\delta^{13}C_{ethane} - \delta^{13}C_{methane}$ values can be used to identify the correlation between carbon isotopes and thermal maturity (Fig. 4). In the southern Jingbian gas field, owing to higher thermal maturity, heavy hydrocarbon gases are cracked, leading to a lower content of heavy hydrocarbon gases than in the northern part (Xia *et al.* 2013; Dai *et al.* 2016a). The carbon isotopic reversal occurs in the southern Jingbian gas field compared with the northern Jingbian gas field (Feng *et al.* 2016; Han *et al.* 2018; Li *et al.* 2018). The $\delta^{13}C_{ethane} - \delta^{13}C_{methane}$ values in the southern part are below zero along the y-axis, revealing a rare phenomenon of $\delta^{13}C_{methane} > \delta^{13}C_{ethane}$. In contrast, the $\delta^{13}C_{ethane} - \delta^{13}C_{methane}$ values in the northern part are above zero ($\delta^{13}C_{methane} < \delta^{13}C_{ethane}$), with no carbon isotopic reversal. The southern and northern parts of Jingbian gas field are similar in geological setting but different in thermal maturity (Li *et al.* 2008; Dai *et al.* 2016a; Feng *et al.* 2016; Han *et al.* 2017a). Therefore, high thermal maturity is hypothesized to be the main reason for the carbon isotopic reversal in southern part of the Jingbian gas field.

Figure 4 suggests that the carbon isotopic reversal occurs with the increase in thermal maturity. However, the impacts of thermal maturity on $\delta^{13}C_{methane}$ and $\delta^{13}C_{ethane}$ values are still unclear.

Solving this issue may provide important clues as to how the thermal maturity induced the carbon isotopic reversal. To clarify the impact of thermal maturity on $\delta^{13}C_{methane}$ and $\delta^{13}C_{ethane}$ values, charts showing the correlation between heavy hydrocarbons (C_{2+}) and $\delta^{13}C_n$ are plotted (Fig. 5).

As we can see from the chart (Fig. 5b), the $\delta^{13}C_{ethane}$ values are obviously different in the southern and northern parts, being much lower in the southern part. In other words, natural gases from the northern Jingbian gas field distribute above the southern Jingbian gas field in the y-axis direction. As mentioned above, the southern and northern parts are similar in geological setting but different in thermal maturity (Li *et al.* 2008; Dai *et al.* 2016a; Feng *et al.* 2016; Han *et al.* 2017a). Therefore, higher thermal maturity leads to relatively lighter $\delta^{13}C_{ethane}$ values in the southern Jingbian gas field. As we can see from Figure 5a, the $\delta^{13}C_{methane}$ values increase with thermal maturity. However, the extent of the increase in $\delta^{13}C_{methane}$ values is obviously less than the extent of the decrease in $\delta^{13}C_{ethane}$ values. This means that when thermal maturity reaches a critical value, its impact on $\delta^{13}C_{methane}$ and $\delta^{13}C_{ethane}$ values is different (Zumberge *et al.* 2012; Xia *et al.* 2013; Han *et al.* 2018). Under the condition of higher thermal maturity (the southern Jingbian gas field), the relationship between thermal maturity and carbon isotope values is no longer consistent with the conventional carbon isotope kinetic fractionation model (Tang *et al.* 2000; Ni & Jin, 2011). When thermal maturity reaches
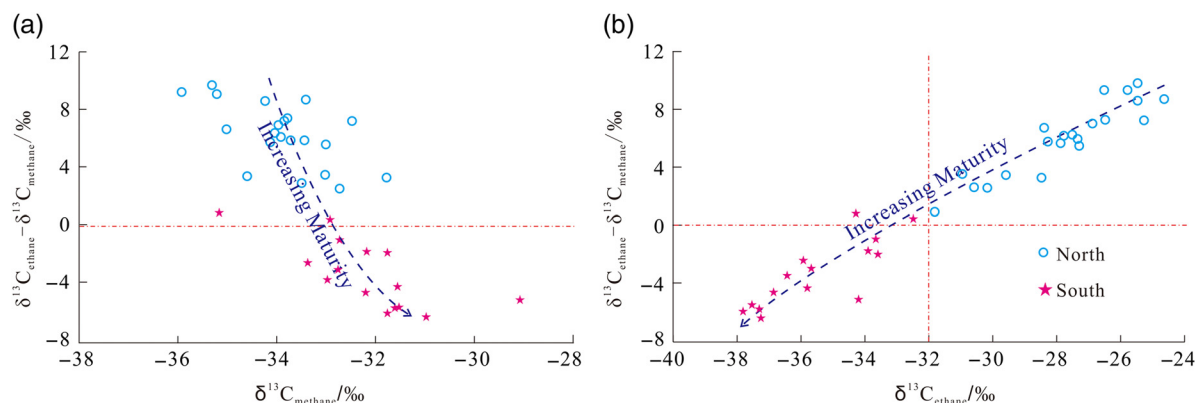
Fig. 6. (Colour online) Relationship between $\delta^{13}C_n$ values and $\delta^{13}C_{ethane} - \delta^{13}C_{methane}$ of natural gas in the northern and southern Jingbian gas field (data from Table 1). (a) $\delta^{13}C_{ethane} - \delta^{13}C_{methane}$ versus $\delta^{13}C_{methane}$; (b) $\delta^{13}C_{ethane} - \delta^{13}C_{methane}$ versus $\delta^{13}C_{ethane}$.
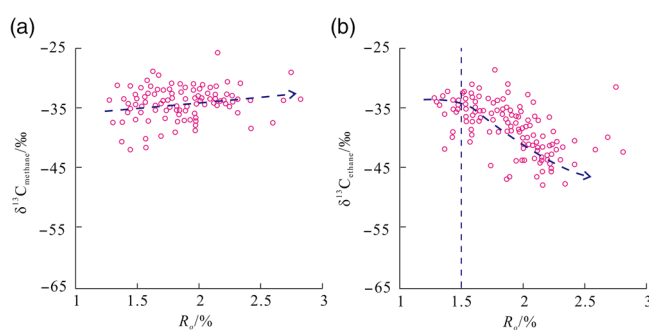
Fig. 7. (Colour online) Relationship between $\delta^{13}C_n$ values and R_o of natural gases in the Ordos Basin (modified after Xia *et al.* 2013).

a critical value (the southern Jingbian gas field), $\delta^{13}C_{ethane}$ values become relatively more depleted with thermal maturity. Although $\delta^{13}C_{methane}$ values increase with thermal maturity, the extent is relatively smaller (Han *et al.* 2018). Finally, the rare phenomenon where $\delta^{13}C_{methane} > \delta^{13}C_{ethane}$ occurs.

$\delta^{13}C_{ethane} - \delta^{13}C_{methane}$ is related to thermal maturity in a negative correlation, and the difference value decreases gradually as thermal maturity increases (Liu *et al.* 2009, 2019; Han *et al.* 2018). A negative difference value indicates a carbon isotopic reversal. The relationship between $\delta^{13}C_n$ and $\delta^{13}C_{ethane} - \delta^{13}C_{methane}$ is plotted to identify the genetic types, thermal maturity and carbon isotopic reversal of the natural gas (Fig. 6). Almost all the gas samples from the southern part show carbon isotopic reversals compared to those from the northern part. The $\delta^{13}C_{ethane}$ values in the northern part are obviously higher than those in the southern part, with no overlaps in the x-axis direction (Fig. 6b). However, in the y-axis direction, from north to south, with the increase in thermal maturity, the $\delta^{13}C_{ethane} - \delta^{13}C_{methane}$ value is gradually less than zero, which suggests carbon isotopic reversal ($\delta^{13}C_{methane} > \delta^{13}C_{ethane}$). High thermal maturity leads to the carbon isotopic reversal of natural gas in the southern part. As mentioned above, when the thermal maturity reaches a critical value, with the increase in thermal maturity, the $\delta^{13}C_{ethane}$ value will become depleted while the $\delta^{13}C_{methane}$ value will continuously increase (Xia *et al.* 2013; Feng *et al.* 2016; Han *et al.* 2018). However, the extent of the increase in $\delta^{13}C_{methane}$ value is smaller than the extent of the decrease in $\delta^{13}C_{ethane}$ value. As shown in Figure 6, the abscissa interval of Figure 6b is obviously wider than that of Figure 6a.

The different impacts of high thermal maturity on $\delta^{13}C_{methane}$ values and $\delta^{13}C_{ethane}$ values will finally lead to a carbon isotopic reversal ($\delta^{13}C_{methane} > \delta^{13}C_{ethane}$).

When the thermal maturity reaches a critical value, it will lead to the cracking of the liquid hydrocarbon generated early and the residual kerogen. The mixing of the cracked gas leads to the carbon isotopic reversal in the southern Jingbian gas field. Other scholars made similar conclusions in their studies of the Ordos Basin. According to Xia *et al.* (2013), high thermal maturity leads to cracking, and the cracked gas then mixes with the primary gas, eventually leading to a carbon isotopic reversal (Fig. 7).

This was also confirmed by the $\delta^{13}C_{ethane} - \delta^{13}C_{propane}$ versus $Ln(C_2H_6/C_3H_8)$ diagram, and the $Ln(C_2H_6/C_3H_8)$ versus $Ln(CH_4/C_2H_6)$ diagram. The diagram identifying the cracked and primary gases was proposed by Prinzhofer & Huc (1995). It is based on the results of Berhar *et al.*'s (1992) simulation experiment, combined with the characteristics of the primary gas of Angola and cracked gas of Kansas. All the gas samples from the Jingbian gas field were plotted onto the diagram, the gases in the south and north distributing in different zones (Fig. 8a). Liu *et al.* (2019) modified and updated the diagram based on data from Chinese basins, including the Turpan-Hami Basin, Sichuan Basin and Liaohe Basin. Gas samples from the Jingbian gas field were also plotted onto this diagram (Fig. 8b). As we can see from the figure, gas samples from the north distribute in the kerogen cracked gas field (refers to primary gases). However, those of the south distribute in the mixed cracked gas and primary gas field. This further confirms that higher
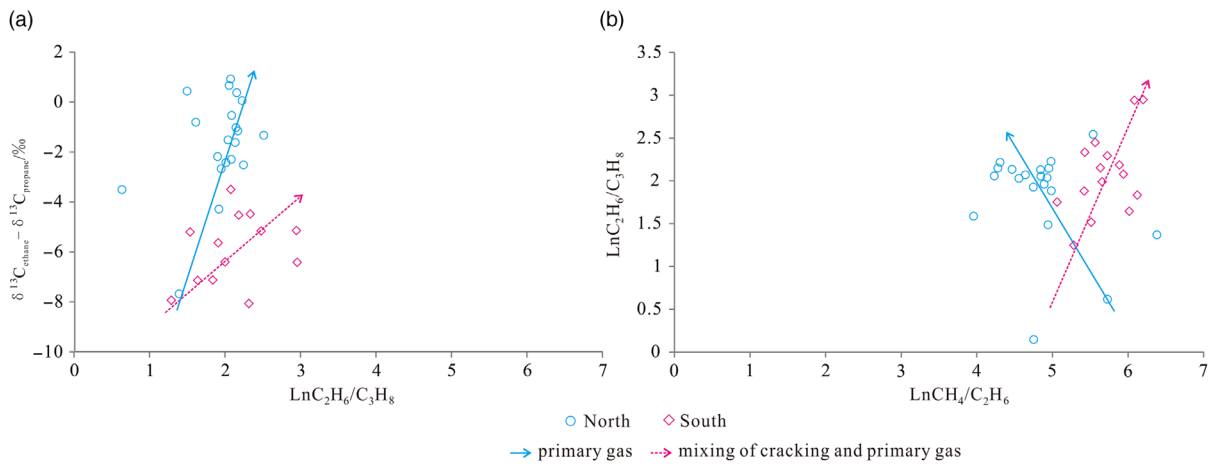
Fig. 8. (Colour online) Relationship between $\delta^{13}C_{ethane} - \delta^{13}C_{propane}$ versus $Ln(C_2H_6/C_3H_8)$ and $Ln(C_2H_6/C_3H_8)$ versus $Ln(CH_4/C_2H_6)$ identifying primary gas and mixed cracked and primary gas (modified after Behar *et al.* 1992; Prinzhofer & Huc, 1995; Liu *et al.* 2019; data from Table 1).
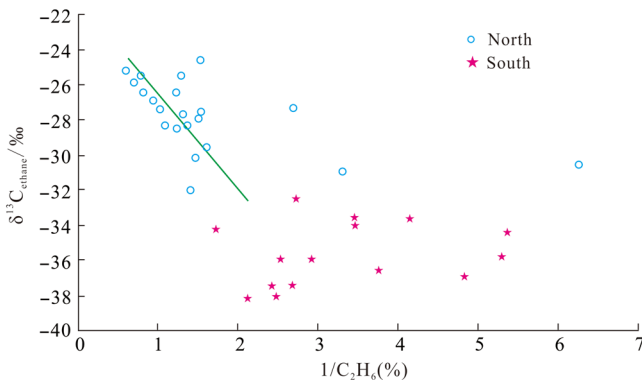
Fig. 9. (Colour online) Relationship between $\delta^{13}C_{ethane}$ values and $1/C_2H_6$ of natural gas in the northern and southern Jingbian gas field (data from Table 1).
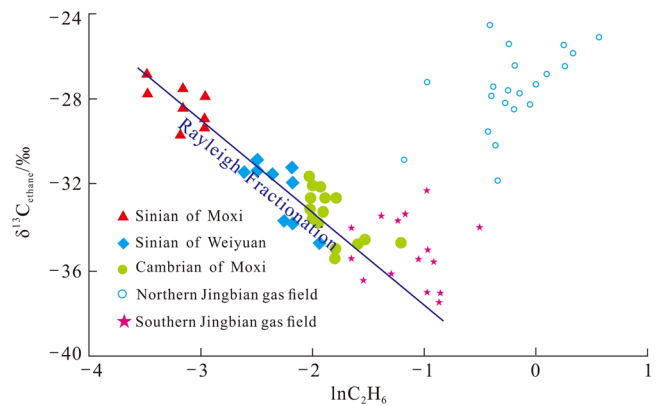
Fig. 10. (Colour online) Relationship between $\delta^{13}C_{ethane}$ values and lnC_2H_6 of natural gas (data for Sichuan Basin from Wu *et al.* 2016; data for Jingbian gas field from Table 1).

thermal maturity causes the cracking of primary gas, and the mixing between primary and cracked gases finally leads to the carbon isotopic reversal in the southern Jingbian gas field of the Ordos Basin.

5.b. Mixing action

Supposing natural gas C is mixed with A and B of different origins, according to the material balance principle, the content of C should conform to the following equation (Jenden *et al.* 1993; Wu *et al.* 2016; Han *et al.* 2018):

$$C_n^C = f_A \times C_n^A + (1 - f_A) \times C_n^B$$

The carbon isotopes should conform to the following equation:

$$\delta^{13}C_n^C = [f_A \times C_n^A \times \delta^{13}C_n^A + (1 - f_A) \times C_n^B \times \delta^{13}C_n^B]/C_n^C$$

When combining the above equations, f_A can be removed to get the following equation:

$$\delta^{13}C_n^C = (C_n^A \delta^{13}C_n^A - C_n^B \delta^{13}C_n^B)/(C_n^A - C_n^B)$$
$$- C_n^A C_n^B (\delta^{13}C_n^A - \delta^{13}C_n^B)/(C_n^A - C_n^B) \times (1/C_n^C)$$

The above equation can be further simplified as:

$$\delta^{13}C_n^C = a/C_n^C + b$$

where, n is the carbon number, C_n^C is the content of C, C_n^A is the content of A, C_n^B is the content of B, f_A is the fraction of A, $\delta^{13}C_n^C$ is the carbon isotope value of C, $\delta^{13}C_n^A$ is the carbon isotope value of A, and $\delta^{13}C_n^B$ is the carbon isotope value of B.

It can be seen from the above equation that for a mixture of gases generated from two different source rocks, there is a linear relationship between carbon isotope values and the reciprocal of the composition content (Coplen *et al.* 1983; Wu *et al.* 2016). Therefore, the chart of correlation between $\delta^{13}C_{ethane}$ and $1/C_2H_6$ can be used to verify the mixing of natural gases in the Jingbian gas field. Natural gas in the northern part conforms to the theoretical model of mixed natural gases with different origins (Fig. 9), which is consistent with the confirmed research results (Li
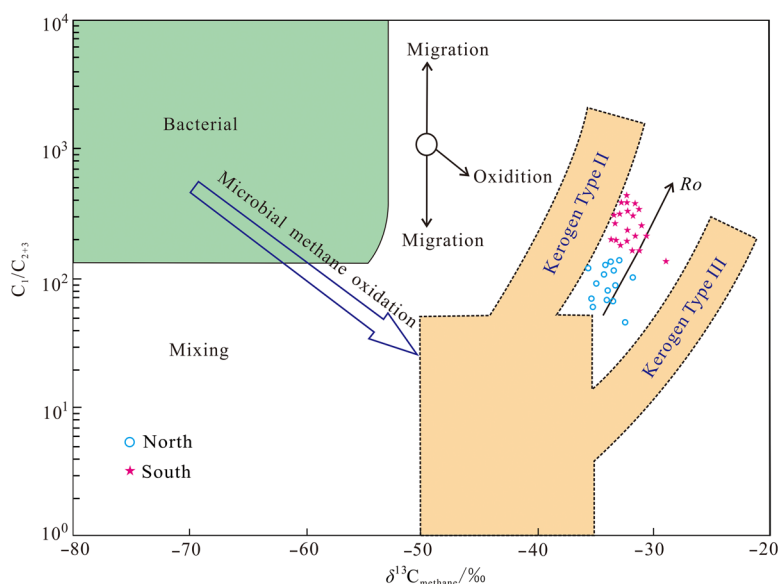
Fig. 11. (Colour online) Relationship between $\delta^{13}C_{methane}$ and C_1/C_{2+3} of natural gas from the northern and southern Jingbian gas field (modified after Bernard *et al.* 1978; Whiticar, 1999; data from Table 1).

etal. 2008; Liu *et al.* 2009; Huang *et al.* 2015; Dai *et al.* 2016*b*; Wang *et al.* 2017*b*).

In contrast, there is no linear relationship between $\delta^{13}C_{ethane}$ and $1/C_2H_6$ in the southern Jingbian gas field. As mentioned above, the southern and northern parts have a similar geologic setting but different thermal maturity (Li *et al.* 2008; Dai *et al.* 2016*a*; Feng *et al.* 2016; Han *et al.* 2017*a*); high thermal maturity is the reason for the abnormal phenomenon. In the southern part, owing to relatively higher thermal maturity, the $\delta^{13}C_{ethane}$ values and $1/C_2H_6$ values deviate from the mixed genetic theory model.

The mixing of organic and inorganic gases could also lead to the carbon isotopic reversal. The Ordos Basin is a stable cratonic basin, and tectonic movements and faults are not developed (Zhao *et al.* 2010; Qiu *et al.* 2015; Dai *et al.* 2016*b*; Wang *et al.* 2017*a*; Guo *et al.* 2018). Therefore, the inorganic mantle gases could not migrate to reservoirs and mix with the organic gases. Dai *et al.* (2017) have also confirmed that the Ordos Basin has no inorganic mantle gas injection. The possibility of the mixture with inorganic mantle gases is excluded.

5.c. Rayleigh fractionation

As the thermal maturity continues to increase, gases may undergo Rayleigh fractionation (Tang *et al.* 2000; Valentine *et al.* 2004; Blaser *et al.* 2015; Laskar *et al.* 2016; Chang *et al.* 2017). In this process, ^{12}C, with bond strengths lower than those of ^{13}C, is cracked in priority. Consequently, the $\delta^{13}C_{ethane}$ values increase gradually in accordance with the following formula (Galimov, 2006):

$$\delta^{13}C_{2,t} = \delta^{13}C_{2,0} - 1000(\alpha - 1)\ln C_{2,0} + 1000(\alpha - 1)\ln C_{2,t}$$

After further processing, the above formula can be simplified as:

$$\delta^{13}C_{2,t} - \delta^{13}C_{2,0} = 1000(\alpha - 1)\ln C_{2,t}/C_{2,0}$$

where, $\delta^{13}C_{2,0}$ is the carbon isotope of primary ethane, ‰; $\delta^{13}C_{2,t}$ is the carbon isotope of ethane after fractionation, ‰; $C_{2,0}$ is the initial ethane content, %; $C_{2,t}$ is the content of ethane after fractionation, %; and α is the carbon isotope fractionation factor.

According to the above formula, a linear relationship can be observed between $\delta^{13}C_{ethane}$ values and contents of ethane during Rayleigh fractionation. In other words, the $\delta^{13}C_{ethane}$ values will gradually increase with the decrease in ethane content. A chart showing the correlation between $\delta^{13}C_{ethane}$ values and $\ln C_2H_6$ is plotted for the southern and northern parts (Fig. 10).

As we can see from Figure 10, there is no negative correlation between $\delta^{13}C_{ethane}$ values and $\ln C_2H_6$ in the Jingbian gas field, which is different from the natural gas of the Cambrian and Sinian systems that experienced Rayleigh fractionation verified in the Chuanzhong Uplift of the Sichuan Basin (Wu *et al.* 2016). Therefore, Rayleigh fractionation does not occur in the natural gas of the Jingbian gas field. The abnormal carbon isotope values of the natural gas of Jingbian gas field are not induced by Rayleigh fractionation.

Owing to higher thermal maturity in the southern Jingbian gas field, heavy hydrocarbon generated early did crack (Xia *et al.* 2013; Dai *et al.* 2016*a*; Feng *et al.* 2016; Wang *et al.* 2017*b*), but the extent of cracking did not reach the stage of Rayleigh fractionation. In other words, if Rayleigh fractionation had occurred, the $\delta^{13}C_{ethane}$ values should gradually increase, but the actual situation is that the $\delta^{13}C_{ethane}$ values in the southern region gradually decrease. Therefore, the southern Jingbian gas field did not experience Rayleigh fractionation.

This can also be confirmed from Figure 11 (Bernard *et al.* 1978; Whiticar, 1999). Gases from the northern and southern Jingbian gas field show the characteristics of thermogenetic gas with the same kerogen type, which suggests that they are generated from the same source rocks (Fig. 11). However, the R_o of the southern part is obviously higher than that of the northern part. It can also be observed that gas samples from both the southern and northern parts do not show the trend of migration fractionation or bacterial oxidation, suggesting that carbon isotopic reversal in the southern Jingbian gas field is not induced by migration fractionation or bacterial oxidation.

6. Conclusions

The Jingbian gas field is divided into southern and northern parts by thermal maturity, with higher maturity in the southern part. For the

southern and northern parts, the interval and mode of the $\delta^{13}C_{methane}$ values are similar, but the $\delta^{13}C_{ethane}$ values are much larger in the northern part than in the southern part. Carbon isotopic reversal ($\delta^{13}C_{methane} > \delta^{13}C_{ethane}$) occurs in the southern part.

Carbon isotopic reversal in the southern part is attributed to higher thermal maturity and mixing between cracked gases and primary gases. When thermal maturity reaches a critical value, $\delta^{13}C_{ethane}$ values becomes relatively more depleted with maturity. Although $\delta^{13}C_{methane}$ values will increase with thermal maturity, the extent will be relatively smaller. Finally, the rare phenomenon where $\delta^{13}C_{methane} > \delta^{13}C_{ethane}$ occurs. High thermal maturity leads to the secondary thermal cracking of the liquid hydrocarbon generated early and the residual kerogen. Mixing of the cracked gases with primary gases also leads to carbon isotopic reversal in the southern part.

Both of the above mechanisms contain a common premise, which is high thermal maturity. High thermal maturity may affect $\delta^{13}C_n$ values. On the other hand, high thermal maturity also leads to cracking, and the mixing of the cracked gases with the primary gases eventually leads to carbon isotopic reversal.

References

Behar F, Kressmann S, Rudkiewicz JL and Vandenbroucke M (1992) Experimental simulation in a confined system and kinetic modelling of kerogen and oil cracking. *Organic Geochemistry* **19**, 173–89.

Bernard BB, Brooks JM and Sackett WM (1978) Light hydrocarbons in recent Texas continental shelf and slope sediments. *Journal of Geophysical Research Oceans* **83**, 4053–61.

Blaser MB, Dreisbach LK and Conrad R (2015) Carbon isotope fractionation of *Thermoanaerobacter kivui* in different growth media and at different total inorganic carbon concentration. *Organic Geochemistry* **81**, 45–52.

Burruss RC and Laughrey CD (2010) Carbon and hydrogen isotopic reversals in deep basin gas: evidence for limits to the stability of hydrocarbons. *Organic Geochemistry* **41**, 1285–96.

Chang XC, Shi BB, Han ZZ and Li TT (2017) C_5–C_{13} light hydrocarbons of crude oils from northern Halahatang oilfield (Tarim Basin, NW China) characterized by comprehensive two-dimensional gas chromatography. *Journal of Petroleum Science and Engineering* **157**, 223–31.

Chung HM, Gormly JR and Squires RM (1988) Origin of gaseous hydrocarbons in subsurface environment: theoretical considerations of carbon isotope distribution. *Chemical Geology* **71**, 97–104.

Coplen TB, Brand WA, Gehre M, Gröning M, Meijer HAJ, Toman B and Verkouteren RM (2006) New guidelines for $\delta^{13}C$ measurements. *Analytical Chemistry* **78**, 2439–41.

Coplen TB, Kendall C and Hopple J (1983) Comparison of stable isotope reference samples. *Nature* **302**, 236–8.

Dai JX, Ni YY, Huang SP, Gong DY, Liu D, Feng ZQ, Peng WL and Han WX (2016a) Secondary origin of negative carbon isotopic series in natural gas. *Journal of Natural Gas Geoscience* **1**, 1–7.

Dai JX, Ni YY, Qin SF, Huang SP, Gong DY, Liu D, Feng ZQ, Peng WL, Han WX and Fang CC (2017) Geochemical characteristics of He and CO_2 from the Ordos (cratonic) and Bohaibay (rift) basins in China. *Chemical Geology* **469**, 192–213.

Dai JX, Song Y, Dai CS and Wang DR (1996) Geochemistry and accumulation of carbon dioxide gases in China. *American Association of Petroleum Geologists Bulletin* **80**, 1615–26.

Dai JX, Xia XY, Li ZS, Coleman DD, Dias RF, Gao L, Li J, Deev A, Li J, Dessort D, Dulerc D, Li LW, Liu JZ, Schloemer S, Zhang WL, Ni YY, Hu GY, Wang XB and Tang YC (2012) Inter-laboratory calibration of natural gas round robins for δ^2H and $\delta^{13}C$ using off-line and on-line techniques. *Chemical Geology* **310–311**, 49–55.

Dai JX, Xia XY, Qin SF and Zhao JZ (2004) Origins of partially reversed alkane $\delta^{13}C$ values for biogenic gases in China. *Organic Geochemistry* **35**, 405–11.

Dai JX, Zou CN, Hu GY, Li W, Li J, Tao SZ, Zhu GY, Ni YY, Yang C, Huang BJ, Shi HS, Huang SP, Zhang WZ, Liu QY, Xie ZY, Li ZS, Qin SF, Li XS, Zhu JZ, Luo X, Zhao ZH, Yang Z, Li J, Wang XB, Jiang XH, Gong YJ, Tao XW, Liao FR, Yu C, Gong DY, Fang CC, Wu W, Meng QQ, Wang J and Liu D (2016b) *Giant Coal-Derived Gas Fields and Their Gas Sources in China*. Beijing, China: Science Press.

Ding WL, Dai P, Zhu DW, Zhang YQ, He JH, Li A and Wang RY (2016) Fractures in continental shale reservoirs: a case study of the Upper Triassic strata in the SE Ordos Basin, Central China. *Geological Magazine* **153**, 663–80.

Du JM, Zhao YD, Wang QC, Yu YQ, Xiao H, Xie XK, Du YG and Su ZM (2019) Geochemical characteristics and resource potential analysis of Chang 7 organic-rich black shale in the Ordos Basin. *Geological Magazine* **156**, 1131–40.

Dumke I, Faber E and Poggenburg R (1989) Determination of stable carbon and hydrogen isotopes of light hydrocarbons. *Analytical Chemistry* **61**, 2149–54.

Fan AP, Yang RC, Lenhardt N, Wang M, Han ZZ, Li JB, Li YJ and Zhao ZJ (2019) Cementation and porosity evolution of tight sandstone reservoirs in the Permian Sulige gas field, Ordos Basin (central China). *Marine and Petroleum Geology* **103**, 276–93.

Fan AP, Yang RC, Loon AJV, Yin W, Han ZZ and Zavala C (2018) Classification of gravity-flow deposits and their significance for unconventional petroleum exploration, with a case study from the Triassic Yanchang Formation (southern Ordos Basin, China). *Journal of Asian Earth Sciences* **161**, 57–73.

Feng ZQ, Liu D, Huang SP, Gong DY and Peng WL (2016) Geochemical characteristics and genesis of natural gas in the Yan'an gas field, Ordos Basin, China. *Organic Geochemistry* **102**, 67–76.

Fuex AA (1977) The use of stable carbon isotopes in hydrocarbon exploration. *Journal of Geochemical Exploration* **7**, 155–88.

Galimov EM (2006) Isotope organic geochemistry. *Organic Geochemistry* **37**, 1200–62.

Guo P, Liu CY, Wang JQ, Deng Y, Mao GZ and Wang WQ (2018) Detrital-zircon geochronology of the Jurassic coal-bearing strata in the western Ordos Basin, North China: evidences for multi-cycle sedimentation. *Geoscience Frontiers* **9**, 1725–43.

Han WX, Ma WJ, Tao SZ, Huang SP, Hou LH and Yao JL (2018) Carbon isotope reversal and its relationship with natural gas origins in the Jingbian gas field, Ordos Basin, China. *International Journal of Coal Geology* **196**, 260–73.

Han WX, Tao SZ, Hou LH and Yao JL (2017a) Geochemical characteristics and genesis of oil-derived gas in the Jingbian gas field, Ordos Basin, China. *Energy and Fuels* **31**, 10432–41.

Han WX, Tao SZ, Hu GY, Ma WJ, Liu D, Feng ZQ and Peng WL (2017b) Light hydrocarbon geochemical characteristics and their application in Upper Paleozoic, Shenmu gas field, Ordos Basin. *Energy Exploration and Exploitation* **35**, 103–21.

He LJ and Zhang LY (2018) Thermal evolution of cratons in China. *Journal of Asian Earth Sciences* **164**, 237–47.

Huang SP, Fang X, Liu D, Fang CC and Huang TF (2015) Natural gas genesis and sources in the Zizhou gas field, Ordos Basin, China. *International Journal of Coal Geology* **152**, 132–43.

Jenden PD, Draza DJ and Kaplan IR (1993) Mixing of thermogenic natural gases in northern Appalachian Basin. *American Association of Petroleum Geologists Bulletin* **77**, 980–98.

Laskar AH, Yadava MG and Ramesh R (2016) Stable and radioactive carbon in forest soils of Chhattisgarh, Central India: implications for tropical soil

carbon dynamics and stable carbon isotope evolution. *Journal of Asian Earth Sciences* **123**, 47–57.

Li Y, Chang XC, Yin W, Sun TT and Song TT (2017) Quantitative impact of diagenesis on reservoir quality of the Triassic Chang 6 tight oil sandstones, Zhenjing area, Ordos Basin, China. *Marine and Petroleum Geology* **86**, 1014–28.

Li J, Li J, Li ZS, Zhang CL, Cui HY and Zhu ZL (2018) Characteristics and genetic types of the Lower Paleozoic natural gas, Ordos Basin. *Marine and Petroleum Geology* **89**, 106–19.

Li H, Ren ZL, Gao HR, Guo DY, Lin J, Li Y, Li CF and Bai N (2015) Quality evaluation and hydrocarbon generation-expulsion characteristics of source rocks in Upper Paleozoic in the Yanchang Gasfield, Ordos Basin. *Natural Gas Industry* **35**, 33–9 (in Chinese with English abstract).

Li J, Zhang WZ, Luo X and Hu GY (2008) Paleokarst reservoirs and gas accumulation in the Jingbian field, Ordos Basin. *Marine and Petroleum Geology* **25**, 401–15.

Liu QY, Chen MJ, Liu WH, Li J, Han PL and Guo YR (2009) Origin of natural gas from the Ordovician paleo-weathering crust and gas-filling model in Jingbian gas field, Ordos Basin, China. *Journal of Asian Earth Sciences* **35**, 74–88.

Liu QY, Worden RH, Jin ZJ, Liu WH, Li J, Gao B, Zhang DW, Hu AP and Yang C (2013) TSR versus non-TSR processes and their impact on gas geochemistry and carbon stable isotopes in Carboniferous, Permian and Lower Triassic marine carbonate gas reservoirs in the Eastern Sichuan Basin, China. *Geochimica et Cosmochimica Acta* **100**, 96–115.

Liu QY, Wu XQ, Wang XF, Jin ZJ, Zhu DY, Meng QQ, Huang SP, Liu JY and Fu Q (2019) Carbon and hydrogen isotopes of methane, ethane, and propane: a review of genetic identification of natural gas. *Earth-Science Reviews* **190**, 247–72.

Liu D, Zhang WZ, Kong QF, Feng ZQ, Fang CC and Peng WL (2016) Lower Paleozoic source rocks and natural gas origins in Ordos Basin, NW China. *Petroleum Exploration and Development* **43**, 591–601.

Lv DW, Wang DD, Li ZX, Liu HY and Li Y (2017) Depositional environment, sequence stratigraphy and sedimentary mineralization mechanism in the coal bed- and oil shale-bearing succession: a case from the Paleogene Huangxian Basin of China. *Journal of Petroleum Science and Engineering* **148**, 32–51.

Ni YY and Jin YB (2011) Carbon isotopic fractionations during Fischer-Tropsch synthesis. *Petroleum Exploration and Development* **38**, 249–56.

Prinzhofer AA and Huc AY (1995) Genetic and post-genetic molecular and isotopic fractionations in natural gases. *Chemical Geology* **126**, 281–90.

Qiu XW, Liu CY, Mao GZ, Deng Y, Wang FF and Wang JQ (2015) Major, trace and platinum-group element geochemistry of the Upper Triassic nonmarine hot shales in the Ordos Basin, Central China. *Applied Geochemistry* **53**, 42–52.

Ren ZL, Yu Q, Cui JP, Qi K, Chen ZJ, Cao ZP and Yang P (2017) Thermal history and its controls on oil and gas of the Ordos Basin. *Earth Science Frontiers* **24**, 137–48 (in Chinese with English abstract).

Ren ZL, Zhang S, Gao SL, Cui JP and Liu XS (2006) Research on region of maturation anomaly and formation time in Ordos Basin. *Acta Geologica Sinica* **80**, 674–84 (in Chinese with English abstract).

Ren ZL, Zhang S, Gao SL, Cui JP, Xiao YY and Xiao H (2007) Tectonic thermal history and its significance on the formation of oil and gas accumulation and mineral deposit in Ordos Basin. *Science in China Series D: Earth Sciences* **50**, 27–38.

Rooney MA, Claypool GE and Chung HM (1995) Modeling thermogenic gas generation using carbon isotope ratios of natural gas hydrocarbons. *Chemical Geology* **126**, 219–32.

Shi BB, Chang XC, Yin W, Li Y and Mao LX (2019) Quantitative evaluation model for tight sandstone reservoirs based on statistical methods – a case study of the Triassic Chang 8 tight sandstones, Zhenjing area, Ordos Basin, China. *Journal of Petroleum Science and Engineering* **173**, 601–16.

Tang Y, Perry JK, Jenden PD and Schoell M (2000) Mathematical modeling of stable carbon isotope ratios in natural gases. *Geochimica et Cosmochimica Acta* **64**, 2673–87.

Tilley B and Muehlenbachs K (2013) Isotope reversals and universal stages and trends of gas maturation in sealed, self-contained petroleum systems. *Chemical Geology* **339**, 194–204.

Valentine DL, Chidthaisong A, Rice A, Reeburgh WS and Tyler SC (2004) Carbon and hydrogen isotope fractionation by moderately thermophilic methanogens 1. *Geochimica et Cosmochimica Acta* **68**, 1571–90.

Wang GW, Chang XC, Yin W, Li Y and Song TT (2017a) Impact of diagenesis on reservoir quality and heterogeneity of the Upper Triassic Chang 8 tight oil sandstones in the Zhenjing area, Ordos Basin, China. *Marine and Petroleum Geology* **83**, 84–96.

Wang K, Pang XQ, Zhao ZF, Wang S., Hu T, Zhang K and Zheng TY (2017b) Geochemical characteristics and origin of natural gas in southern Jingbian gas field, Ordos Basin, China. *Journal of Natural Gas Science and Engineering* **46**, 515–25.

Wang DD, Shao LY, Li ZX, Li MP, Lv DW and Liu HY (2016) Hydrocarbon generation characteristics, reserving performance and preservation conditions of continental coal measure shale gas: a case study of Mid-Jurassic shale gas in the Yan'an Formation, Ordos Basin. *Journal of Petroleum Science and Engineering* **145**, 609–28.

Wang ZT, Zhou HR, Wang XL, Jing XC and Zhang YS (2015) Volcanic event records at the southwestern Ordos Basin: the message from geochemical and zircon U–Pb geochronology of K-bentonites from Pingliang Formation, Shaanxi and Gansu region. *Acta Petrologica Sinica* **31**, 2633–54 (in Chinese with English abstract).

Whiticar MJ (1999) Carbon and hydrogen isotope systematics of bacterial formation and oxidation of methane. *Chemical Geology* **161**, 291–314.

Wu W, Dong DZ, Yu C and Liu D (2015) Geochemical characteristics of shale gas in Xiasiwan area, Ordos Basin. *Energy Exploration & Exploitation* **33**, 25–42.

Wu XQ, Liu QY, Zhu JH, Li K, Liu GX, Chen YB and Ni CJ (2017) Geochemical characteristics of tight gas and gas-source correlation in the Daniudi gas field, the Ordos Basin, China. *Marine and Petroleum Geology* **79**, 412–25.

Wu W, Luo C, Zhang J and Liu WP (2016) Evolution law and genesis of ethane carbon isotope of oil type gas. *Acta Petrolei Sinica* **37**, 1463–71 (in Chinese with English abstract).

Xia XY, Chen J, Braun R and Tang YC (2013) Isotopic reversals with respect to maturity trends due to mixing of primary and secondary products in source rocks. *Chemical Geology* **339**, 205–12.

Xiao QL (2012) Carbon and hydrogen isotopic reversals in deep basin gas: Evidence for limits to the stability of hydrocarbons by Burruss and Laughrey (Organic Geochemistry 41, 1285–1296) – Discussion. *Organic Geochemistry* **44**, 71–6.

Xu QH, Shi WZ, Xie XY, Manger W, Mcguire P, Zhang XM, Wang R and Xu Z (2016) Deep-lacustrine sandy debrites and turbidites in the lower Triassic Yanchang Formation, southeast Ordos Basin, central China: facies distribution and reservoir quality. *Marine and Petroleum Geology* **77**, 1098–107.

Yang RC, Fan AP, Han ZZ and Loon AJV (2017) Lithofacies and origin of the Late Triassic muddy gravity-flow deposits in the Ordos Basin, central China. *Marine and Petroleum Geology* **85**, 194–219.

Yang RC, He ZL, Qiu GQ, Jin ZJ, Sun DS and Jin XH (2014) A Late Triassic gravity flow depositional system in the southern Ordos Basin. *Petroleum Exploration and Development* **41**, 724–33.

Yang H, Zhang WZ, Liu XS and Meng PL (2012) Accumulation conditions and exploration and development of tight gas in the Upper Paleozoic of the Ordos Basin. *Petroleum Exploration and Development* **39**, 315–24.

Zhang K (1989) *Tectonics and Resources of Ordos Fault-Block.* Xi'an: Shaanxi Science and Technology Press.

Zhang T and Krooss BM (2001) Experimental investigation on the carbon isotope fractionation of methane during gas migration by diffusion through sedimentary rocks at elevated temperature and pressure. *Geochimica et Cosmochimica Acta* **65**, 2723–42.

Zhang SQ, Wu LJ, Guo JM, Chen XB, Zhao JX, Ding WY, Huang CL, Zhang C and Chen ZT (1985) An interpretation of the dss data on Menyuan-Pingling-Weinan profile in west China. *Acta Geophysica Sinica* **28**, 460–72 (in Chinese with English abstract).

Zhang WZ, Yang H, Peng PA, Yang YH, Zhang H and Shi XH (2009) The Influence of Late Triassic volcanism on the development of Chang 7 high grade hydrocarbon source rock in Ordos Basin. *Geochimica* **38**, 573–82 (in Chinese with English abstract).

Zhao GC, Wilde SA, Guo JH, Cawood PA, Sun M and Li XP (2010) Single zircon grains record two Paleoproterozoic collisional events in the North China Craton. *Precambrian Research* **177**, 266–76.

Zhou Y, Ji YL, Xu LM, Che SQ, Niu XB, Wan L, Zhou YQ, Li ZC and You Y (2016) Controls on reservoir heterogeneity of tight sand oil reservoirs in Upper Triassic Yanchang Formation in Longdong Area, southwest Ordos Basin, China: implications for reservoir quality prediction and oil accumulation. *Marine and Petroleum Geology* **78**, 110–35.

Zou CN, Tao SZ, Han WX, Zhao ZY, Ma WJ, Li CW, Bai B and Gao XH (2018) Geological and geochemical characteristics and exploration prospect of coal-derived tight sandstone gas in China: case study of the Ordos, Sichuan, and Tarim Basins. *Acta Geologica Sinica (English Edition)* **92**, 1609–26.

Zumberge J, Ferworn K and Brown S (2012) Isotopic reversal ('rollover') in shale gases produced from the Mississippian Barnett and Fayetteville formations. *Marine and Petroleum Geology* **31**, 43–52.